Journal of Molecular Structure 1214 (2020) 128023

Contents lists available at ScienceDirect

Journal of Molecular Structure

journal homepage: http://www.elsevier.com/locate/molstruc

High-resolution rovibrational spectroscopy of c-$C_3H_2^+$: The ν_7 C–H antisymmetric stretching band

Oskar Asvany [a, *], Charles R. Markus [a, b], Thomas Salomon [a], Philipp C. Schmid [a], Shreyak Banhatti [a], Sandra Brünken [c], Filippo Lipparini [d, e], Jürgen Gauss [d], Stephan Schlemmer [a]

[a] I. Physikalisches Institut, Universität zu Köln, Zülpicher Str. 77, 50937, Köln, Germany
[b] Department of Chemistry, University of Illinois, Department of Chemistry, Urbana, IL 61801, USA
[c] Radboud University, Institute for Molecules and Materials, FELIX Laboratory, Toernooiveld 7, 6525ED, the Netherlands
[d] Department Chemie, Johannes Gutenberg-Universität Mainz, Duesbergweg 10-14, D-55128, Mainz, Germany
[e] Dipartimento di Chimica e Chimica Industriale, Università di Pisa, Via G. Moruzze 13, I-56124, Pisa, Italy

ARTICLE INFO

Article history:
Received 31 December 2019
Received in revised form
2 March 2020
Accepted 5 March 2020
Available online 13 March 2020

Keywords:
Ion trap
Rovibrational spectroscopy
Action spectroscopy
Coupled cluster calculations
c-$C_3H_2^+$

ABSTRACT

The ν_7 antisymmetric C–H stretching fundamental of c-$C_3H_2^+$ has been characterized in a cryogenic 22-pole ion trap by a novel type of action spectroscopy, in which the rovibrational excitation of c-$C_3H_2^+$ is detected as a slowing down of the low-temperature reaction c-$C_3H_2^+ + H_2 \rightarrow C_3H_3^+ + H$. Ninety-one rovibrational transitions with partly resolved fine structure doublets were measured in high resolution. Supported by high-level quantum chemical calculations, spectroscopic parameters were determined by fitting the observed lines with an effective Hamiltonian for an asymmetric rotor in a doublet electronic ground state, $\tilde{X}\ ^2A_1$, yielding a band origin at 3113.6400(3) cm^{-1}. Based on these spectroscopic parameters, the rotational spectrum of this astronomically important molecule is predicted.

1. Introduction

The cyclopropenylidene cation, c-$C_3H_2^+$, together with its linear form, $HCCCH^+$, is thought to be an important ingredient in the hydrocarbon chemistry of the interstellar medium, in particular in photon-dominated regions (PDRs). Together with isomeric forms of $C_3H_3^+$ they are formed through hydrogen abstraction or association reactions of C_3H^+ in collision with molecular hydrogen, and they can dissociatively recombine with an electron to produce neutral hydrocarbons, leading, e.g., to C_3H and C_3H_2, which are ubiquitous in both diffuse and dark cloud cores [1,2]. While this scenario is well proven by laboratory-spectroscopy based astronomical detection of the neutrals l/c-C_3H [3–5], l/c-C_3H_2 [6,7], and the cation l-C_3H^+ [8,9], the important reaction intermediates $C_3H_2^+$ and $C_3H_3^+$ still await astronomical detection. The latter ion has been investigated in its cyclic form by high-resolution rovibrational spectroscopy in the laboratory [10], but its missing permanent dipole moment prohibits a radio-astronomical observation. Further clues about the intrinsic details of this chemistry network may be provided by the $C_3H_2^+$ species, for which high-resolution laboratory data has been so far missing.

Spectroscopic information on $C_3H_2^+$ has been very sparse. For a long time, photoelectron spectroscopy of neutral c-C_3H_2 was the only source of coarse vibrational information on the cation [11,12]. Very recently, the Ne-tagged linear and cyclic forms of $C_3H_2^+$ were investigated in low resolution with the FELion instrument [13] at the FELIX facility [14], detecting all IR active vibrational fundamentals of c-$C_3H_2^+$. In particular, the intense ν_7 antisymmetric C–H stretching band of c-$C_3H_2^+$ has been located at 3116 cm^{-1} [15].

Based on this information and results from quantum chemical calculations of the rotational structure, in this work we characterized the ν_7 fundamental of c-$C_3H_2^+$ in high resolution. For the action spectroscopic detection scheme, named Laser Induced Hindering of a Reaction (LIHR) [16], the low-temperature collision [17]

$$c - C_3H_2^+ + H_2 \rightarrow c - C_3H_3^+ + H \quad (1)$$

* Corresponding author.
E-mail address: asvany@ph1.uni-koeln.de (O. Asvany).

https://doi.org/10.1016/j.molstruc.2020.128023
0022-2860/

has been exploited as an indicator for the rovibrational excitation of c-$C_3H_2^+$. This action scheme is based on the fact that the rate coefficient of this reaction has a negative temperature dependence [18], being slow at low temperature (1.7×10^{-13} cm^3s^{-1} at 15 K), and even slower for hot, i.e., excited, reaction partners. With the ninety-one rovibrational transitions measured in this work, we were able to determine the ground state spectroscopic parameters and to predict the rotational spectrum of c-$C_3H_2^+$.

2. Experimental setup

The experiments have been carried out in the cryogenic 22-pole ion trapping machine COLTRAP [19]. The c-$C_3H_2^+$ ions have been generated in a storage ion source by electron impact ionization ($E_e \approx$ 30 eV) of a 3:1 mixture of helium (Linde 5.0) and allene (C_3H_4, abcr GmbH, 96%). This precursor is known to yield the cyclic and linear isomers of $C_3H_2^+$ in a ratio of about 60:40 under conditions prevailing in our ion source [15]. A pulse of several ten thousand ions was selected in a quadrupole mass spectrometer for mass 38 u and then injected into the 22-pole ion trap [20]. The trap was held at about $T =$ 9 K and was constantly filled with approximately 3×10^{11} cm^{-3} of hydrogen (Linde 6.0) for reaction (1) to proceed. During the trapping time of typically 400 ms the cold $C_3H_2^+$ ion ensemble was irradiated with narrow-bandwidth IR radiation, provided by a continuous-wave optical parametric oscillator (Aculight Argos Model 2400 module C) operated in the 3 μm range. Its narrow beam was crossing the 22-pole ion trap, with power on the order of 100 mW. The frequency of the infrared (IR) radiation was measured by a wavemeter (Bristol model 621A) with an accuracy of about 0.001 cm^{-1}. After the trapping period, the trap content was extracted, selected in a second quadrupole mass spectrometer for the reaction product $C_3H_3^+$ (mass 39 u), and counted in a high-efficiency ion counter. By repeating these trapping cycles every second and counting the $C_3H_3^+$ ions as a function of the IR wavenumber, several narrow spectral features around the predicted position of the ν_7 mode have been found. These turned out to be rovibrational lines of c-$C_3H_2^+$ as confirmed by the spectroscopic analysis given below.

3. Quantum chemical calculations

High-level quantum chemical calculations at the coupled cluster (CC) level [21] have been carried out in order to predict the relevant spectroscopic parameters of c-$C_3H_2^+$ and in order to support the assignment and analysis of the experimental data.

For this, the geometry of c-$C_3H_2^+$ has been optimized in a first step at the CC singles and doubles (CCSD) level [22] augmented by a pertubative treatment of triple excitations (CCSD(T)) [23] using various choices from Dunning's hierarchy of correlation consistent basis sets [24,25] and using analytically evaluated forces [26], thereby using an unrestricted Hartree-Fock (HF) reference function in the CC treatment. To be more specific, geometry optimizations have been carried out at the frozen-core (fc) CCSD(T)/cc-pVTZ level ($r(C_1C_1') = 1.40148$ Å, $r(C_1C_2) = 1.36000$ Å, $r(C_1H) = 1.08248$ Å, $\langle(HC_1C_1') = 146.59°$) and the all-electron CCSD(T)/cc-pCVQZ level ($r(C_1C_1') = 1.39312$ Å, $r(C_1C_2) = 1.35159$ Å, $r(C_1H) = 1.08055$ Å, $\langle(HC_1C_1') = 146.63°$). The equilibrium geometry of c-$C_3H_+^2$ has been further refined by using a composite scheme combined with basis-set extrapolation [27,28] in order to account for higher-order correlation effects, i.e., the full treatment of triple excitations (using the cc-pVTZ basis and within the frozen-core approximation) as well as quadruple excitations (using the cc-pVDZ basis and within the frozen-core approximation) and to provide results close to the basis set limit (extrapolations were done at the HF level using cc-pVXZ, X = Q,5,6 and at the frozen-core CCSD(T) level using cc-pVXZ, X = 5,6, core correlation was treated separately at the CCSD(T)/cc-pCV5Z level). The geometry obtained in this way ($r(C_1C_1') = 1.39187$ Å, $r(C_1C_2) = 1.35048$ Å, $r(C_1H) = 1.08031$ Å, $\langle(HC_1C_1') = 146.61°$) can be referred to as theoretical best estimate and is used to provide high-accuracy results for the equilibrium rotational constants of c-$C_3H_2^+$. The CCSD(T)/cc-pCVQZ geometry has been then used as a starting point for a harmonic frequency calculation (thereby employing analytically evaluated second derivatives [29,30]) that yields beside the harmonic vibrational frequencies also the quartic centrifugal distortion constants. The fc-CCSD(T)/cc-pVTZ geometry has been used to carry out a second-order vibrational perturbation theory (VPT2) [31] calculation in order to provide anharmonic corrections to the vibrational frequencies as well as vibrational corrections for the rotational constants of c-$C_3H_2^+$. The VPT2 computation has been carried out as described in Ref. [32] by using a four-point numerical differentiation scheme together with a step size of 0.04 along the reduced normal coordinates to obtain the cubic and quartic force constants from analytically evaluated second derivatives. The electron spin-rotation tensor ε_{ij} has been computed as described in Ref. [33] at the fc-CCSD(T)/cc-pVTZ level using the CCSD(T)/cc-pCVQZ optimized geometry.

All calculations have been carried out using the CFOUR quantum chemical program package [34].

4. Spectroscopic properties of c-$C_3H_2^+$

The c-$C_3H_2^+$ ion has C_{2v} symmetry and a single unpaired electron. Its ground state is $\tilde{X}\ ^2A_1$. The effective Hamiltonian for the analysis of the spectrum is composed of the terms for the rotational energy of an asymmetric top, the spin-rotation interaction $H_{SR} = \varepsilon_{ij}\ N_iS_j$, and the hyperfine interaction (which is not resolved in the current work). The spin-rotation interaction (fine structure) is given by coupling the total electron spin S with the rotational angular momentum N to yield the angular momentum $J = S + N$. Because $S = 1/2$, each rotational level splits into the fine structure doublets $J = N + 1/2$ (F_1) and $N - 1/2$ (F_2). For the lowest energy region the energy level diagram is given in Fig. 1. As c-C_3H_2+ has two hydrogen nuclei with nuclear spins $I_H = 1/2$, its quantum levels can be divided into ortho (total nuclear spin $I = 1$) and para

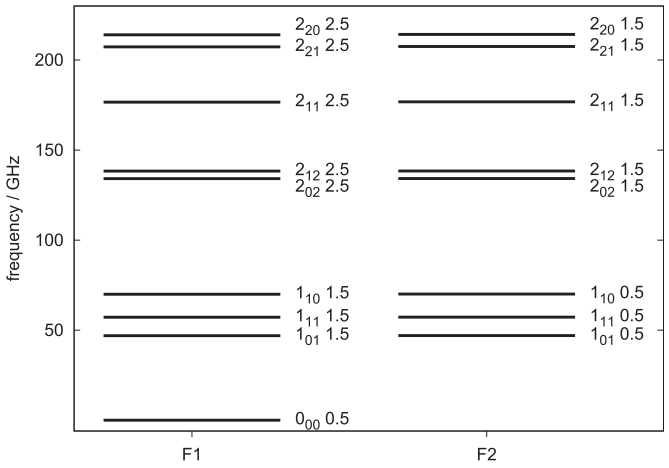

Fig. 1. Schematic diagram showing the lowest fine structure states of c-$C_3H_2^+$, sorted by its components F_1 ($J = N + 1/2$) and F_2 ($J = N - 1/2$). The levels are labeled $N_{K_aK_c}J$. The small hyperfine splittings are not discernible on this energy scale.

(total nuclear spin $I = 0$) species with a statistical weight of 3:1. The ortho-levels ($I = 1$) in the ground vibrational state are those with $K_a + K_c$ odd, and the para-levels ($I = 0$) in the ground vibrational state are those with $K_a + K_c$ even. In the $\nu_7 = 1$ state (b_2 symmetry), these assignments are reversed (i.e. para-states have $K_a + K_c$ odd and ortho-states have $K_a + K_c$ even).

5. Rovibrational spectroscopy of c-$C_3H_2^+$

c-$C_3H_2^+$ has 9 vibrational modes, of which all except ν_5 are IR active. We chose the intense antisymmetric C—H stretching band ν_7 (a-type transition with vibrational symmetry b_2) as our target as it is in the range of our 3 μm OPO. Based on the available vibrational information [15] and our quantum chemical calculations of the rotational structure, we searched the region around 3116 cm^{-1} for spectroscopic signals of c-$C_3H_2^+$ using reaction (1) as the indicator. Soon, reproducible rovibrational lines like the ones depicted in Fig. 2 were found.

These lines sometimes exhibit shoulders, which turn out to be caused by the small fine structure splitting, whereas the hyperfine splitting for the ortho-lines ($I = 1$) can not be resolved in the present experiment. Because of these merged doublets, it is difficult to determine the kinetic temperature of the ions by their Doppler widths. Using lines which appeared narrow, we estimate the kinetic temperature to be in the range of $T_{kin} = 15$ K. In total, 91 lines could be retrieved. The frequencies and intensities of the observed transitions are summarized in Fig. 3 and assigned in Table 1. The lines with highest intensity in Fig. 3 are all ortho-lines due to their higher nuclear spin statistical weight (ortho/para = 3:1).

6. Determination of spectroscopic parameters

In order to determine the spectroscopic parameters, the observed transition frequencies listed in Table 1 have been fitted to an $A-$ reduced Watson-type Hamiltonian including spin-rotation interaction for the ground and $\nu_7 = 1$ states using the program PGOPHER [35]. Initial guesses for the rotational, distortion and spin-rotation constants were provided by our calculations, and were accurate enough to make initial assignments. For transitions which had resolved fine structure, the relative intensities enabled straightforward assignment of the F_1 and F_2 components, for which the F_1 component should be stronger. Transitions where the fine

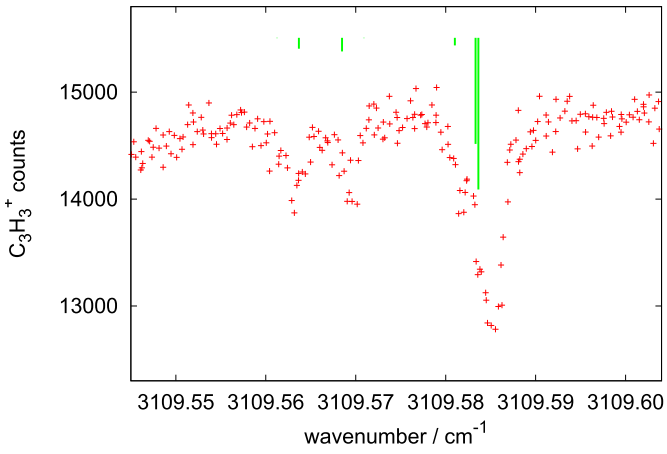

Fig. 2. An example of action spectroscopy of c-$C_3H_2^+$, detected as a dip in the $C_3H_3^+$ counts. The strong transition is the doublet consisting of $N_{K_aK_c}J = 2_{02}2.5 \leftarrow 3_{03}3.5$ (F_1) and its left shoulder $2_{02}1.5 \leftarrow 3_{03}2.5$ (F_2). The green bars are PGOPHER [35] simulations of the fine structure components.

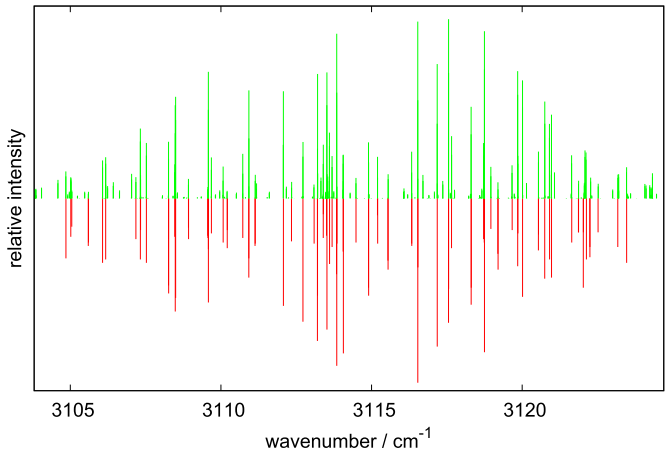

Fig. 3. Stick spectrum overview of the ν_7 band of c-$C_3H_2^+$ comparing the measured rovibrational lines (lower part, red) against the PGOPHER [35] simulation (upper part, green). An intensity fit with PGOPHER yields a rotational temperature $T_{rot} = 20.5 \pm 2.5$ K.

structure was not resolved were fit by treating the two components as an intensity weighted average. Given that the transitions were a-type and the uncertainty of the wavemeter was approximately 0.001 cm^{-1}, only the Δ_N centrifugal distortion term could be determined, which was constrained to be the same for the ground and $\nu_7 = 1$ vibrational state. All other distortion terms and the spin-rotation constants were held at the calculated values, since releasing them did not improve the fit. The final parameters from the fit are summarized in Table 2. It is worth noting that the determined parameters agree remarkably well with the computed ones, which demonstrates the high accuracy of the quantum chemical calculations.

The observed spectrum is compared with the simulated one in Fig. 3. In this simulation, some line positions could not be reproduced well, suggesting that part of the ν_7 band may be perturbed. For example, the transition 7_{17} 6.5 ← 6_{16} 5.5 at 3122.0276 cm^{-1} shows the largest deviation of 0.0561 cm^{-1} from the simulation. Such transitions were excluded from the fit, with missing o-c values in Table 1. In order to confirm assignments and to assess the quality of the ground state parameters, combination differences (CDs) were calculated using transitions which had resolved fine structure and shared a final rovibrational state. In total, 11 combination differences could be determined, which agreed with the values calculated from Table 2 with a root mean square value of 0.00136 cm^{-1}.

7. Predicted rotational spectrum of c-$C_3H_2^+$

Based on the obtained spectroscopic parameters given in Table 2, the rotational spectrum of c-$C_3H_2^+$ has been predicted. A collection of the most intense rotational lines up to 400 GHz is given in Table 3 and the predicted spectrum is summarized in Fig. 4. The c-$C_3H_2^+$ ion has a sufficiently large permanent dipole moment predicted to be around 1.6 Debye (CCSD(T)/cc-pCVQZ calculation, defined with respect to the center of mass as origin), permitting the rotational detection in the laboratory and space.

For the laboratory search of the rotational lines, we applied two different action spectroscopic methods. With the first method, we applied a double-resonance (DR) technique in which the rovibrational spectroscopy described in section 5 is extended by a rotational transition, similar to other DR techniques developed in the Cologne group [36–39]. This search was conducted at a nominal trap temperature of about 9 K. Prime targets were strong rotational

Table 1
Measured rovibrational transitions in the ν_7 C–H antisymmetric stretch fundamental of c-$C_3H_2^+$. The frequencies are given in cm^{-1} and the measured depletion intensities are in (negative) arbitrary units. The uncertainty is 0.001 cm −1 = 30 MHz, which is given by the wavemeter. Transitions which were not included in the fit are listed without an observed - calculated value.

$N'_{K'_aK'_c} \leftarrow N''_{K''_aK''_c}$	$J'-J''$	This work	Obs-Calc	Intensity
$4_{22} \leftarrow 5_{23}$	–	3104.8536	0.0019	−0.053
$6_{06} \leftarrow 7_{07}$	–	3105.0165	0.0024	−0.034
$2_{02} \leftarrow 3_{21}$	2.5–3.5	3105.5980	0.0023	−0.042
$2_{02} \leftarrow 3_{21}$	1.5–2.5	3105.6026	−0.0003	−0.039
$4_{13} \leftarrow 5_{14}$	–	3106.0722	0.0012	−0.057
$5_{15} \leftarrow 6_{16}$	–	3106.1728	−0.0014	−0.054
$3_{12} \leftarrow 4_{13}$	–	3107.1776	0.0009	−0.036
$4_{04} \leftarrow 5_{05}$	–	3107.3250	−0.0010	−0.054
$4_{14} \leftarrow 5_{15}$	–	3107.3317	−0.0015	−0.028
$3_{22} \leftarrow 4_{23}$	–	3107.5270	0.0008	−0.057
$2_{20} \leftarrow 3_{21}$	1.5–2.5	3108.2606	0.0015	−0.077
$2_{20} \leftarrow 3_{21}$	2.5–3.5	3108.2632	0.0017	−0.084
$3_{03} \leftarrow 4_{04}$	–	3108.4672	0.0000	−0.034
$2_{11} \leftarrow 3_{12}$	–	3108.4841	0.0017	−0.100
$3_{13} \leftarrow 4_{14}$	–	3108.4970	−0.0003	−0.088
$2_{21} \leftarrow 3_{22}$	1.5–2.5	3108.9210	0.0012	−0.026
$2_{21} \leftarrow 3_{22}$	2.5–3.5	3108.9242	0.0012	−0.036
$4_{04} \leftarrow 4_{23}$	4.5–4.5	3109.5636	0.0011	−0.033
$4_{04} \leftarrow 4_{23}$	3.5–3.5	3109.5693	−0.0001	−0.035
$2_{02} \leftarrow 3_{03}$	1.5–2.5	3109.5828	−0.0008	−0.045
$2_{02} \leftarrow 3_{03}$	2.5–3.5	3109.5852	0.0002	−0.092
$2_{12} \leftarrow 3_{13}$	–	3109.6842	−0.0006	−0.031
$1_{10} \leftarrow 2_{11}$	–	3110.0735	0.0020	−0.039
$5_{24} \leftarrow 5_{23}$	5.5–5.5	3110.2089	−0.0037	−0.044
$5_{24} \leftarrow 5_{23}$	4.5–4.5	3110.2134	−0.0029	−0.028
$1_{01} \leftarrow 2_{02}$	–	3110.7261	0.0010	−0.035
$1_{11} \leftarrow 2_{12}$	0.5–1.5	3110.9247	−0.0021	−0.053
$1_{11} \leftarrow 2_{12}$	1.5–2.5	3110.9273	−0.0026	−0.070
$3_{13} \leftarrow 3_{12}$	3.5–3.5	3111.1337	−0.0012	−0.042
$3_{13} \leftarrow 3_{12}$	2.5–2.5	3111.1383	−0.0014	−0.040
$0_{00} \leftarrow 1_{01}$	–	3112.0734	0.0006	−0.095
$2_{12} \leftarrow 2_{11}$	–	3112.3416	−0.0027	−0.038
$3_{22} \leftarrow 3_{21}$	–	3112.7237	0.0006	−0.109
$4_{32} \leftarrow 4_{31}$	–	3113.0931	−0.0000	−0.040
$1_{11} \leftarrow 1_{10}$	1.5–1.5	3113.2043	−0.0027	−0.126
$1_{11} \leftarrow 1_{10}$	0.5–0.5	3113.2072	−0.0019	−0.086
$2_{21} \leftarrow 2_{20}$	–	3113.3973	−0.0008	−0.035
$3_{31} \leftarrow 3_{30}$	–	3113.5178	0.0003	−0.116
$4_{40} \leftarrow 4_{41}$	–	3113.6076	0.0007	−0.058
$3_{30} \leftarrow 3_{31}$	–	3113.6901	0.0005	−0.043
$2_{20} \leftarrow 2_{21}$	1.5–2.5	3113.8393	0.0019	−0.067
$2_{20} \leftarrow 2_{21}$	–	3113.8456	0.0006	−0.148
$2_{20} \leftarrow 2_{21}$	2.5–1.5	3113.8512	−0.0013	−0.040
$1_{10} \leftarrow 1_{11}$	–	3114.0590	−0.0016	−0.047
$4_{31} \leftarrow 4_{32}$	–	3114.0635	0.0008	−0.137
$3_{21} \leftarrow 3_{22}$	–	3114.4843	0.0006	−0.039
$2_{11} \leftarrow 2_{12}$	1.5–1.5	3114.9005	−0.0002	−0.079
$2_{11} \leftarrow 2_{12}$	2.5–2.5	3114.9032	−0.0009	−0.086
$1_{01} \leftarrow 0_{00}$	–	3115.2021	0.0007	−0.040
$4_{22} \leftarrow 4_{23}$	3.5–3.5	3115.5451	−0.0037	−0.055
$4_{22} \leftarrow 4_{23}$	4.5–4.5	3115.5473	−0.0039	−0.063
$2_{12} \leftarrow 1_{11}$	2.5–1.5	3116.3327	0.0006	−0.040
$2_{12} \leftarrow 1_{11}$	1.5–0.5	3116.3354	0.0002	−0.042
$2_{02} \leftarrow 1_{01}$	2.5–1.5	3116.5358	0.0009	−0.163
$2_{02} \leftarrow 1_{01}$	1.5–0.5, 1.5–1.5	3116.5389	0.0030	−0.061
$2_{11} \leftarrow 1_{10}$	–	3117.1821	0.0002	−0.131
$3_{13} \leftarrow 2_{12}$	3.5–2.5	3117.5558	−0.0005	−0.110
$3_{13} \leftarrow 2_{12}$	2.5–1.5	3117.5586	0.0002	−0.080
$3_{03} \leftarrow 2_{02}$	–	3117.6561	−0.0000	−0.044
$3_{22} \leftarrow 2_{21}$	3.5–2.5	3118.3063	0.0001	−0.094
$3_{22} \leftarrow 2_{21}$	2.5–1.5	3118.3096	0.0001	−0.079
$4_{14} \leftarrow 3_{13}$	–	3118.7178	−0.0006	−0.036
$3_{12} \leftarrow 2_{11}$	–	3118.7421	0.0008	−0.039
$4_{04} \leftarrow 3_{03}$	–	3118.7469	−0.0010	−0.136
$3_{21} \leftarrow 2_{20}$	–	3118.9613	0.0012	−0.027
$2_{20} \leftarrow 1_{01}$	1.5–0.5, 1.5–1.5	3119.1931	0.0009	−0.049
$2_{20} \leftarrow 1_{01}$	2.5–1.5	3119.2004	−0.0002	−0.063
$4_{23} \leftarrow 3_{22}$	–	3119.6681	0.0003	−0.028
$5_{15} \leftarrow 4_{14}$	–	3119.8506	0.0003	−0.060
$5_{05} \leftarrow 4_{04}$	–	3119.8578	0.0006	−0.031

Table 1 (*continued*)

$N'_{K'_aK'_c} \leftarrow N''_{K''_aK''_c}$	$J'-J''$	This work	Obs-Calc	Intensity
$4_{13} \leftarrow 3_{12}$	–	3120.0125	0.0012	−0.087
$4_{31} \leftarrow 3_{30}$	4.5–3.5	3120.5375	0.0008	−0.046
$4_{31} \leftarrow 3_{30}$	3.5–2.5	3120.5408	0.0008	−0.032
$4_{22} \leftarrow 3_{21}$	–	3120.7480	0.0010	−0.071
$5_{24} \leftarrow 4_{23}$	–	3120.9101	−0.0026	−0.054
$6_{06} \leftarrow 5_{05}$	–	3120.9749	0.0026	−0.070
$5_{33} \leftarrow 4_{32}$	–	3121.6458	−0.0016	−0.039
$5_{42} \leftarrow 4_{41}$	5.5–4.5	3121.8672	−0.0006	−0.030
$5_{42} \leftarrow 4_{41}$	4.5–3.5	3121.8706	−0.0010	−0.030
$7_{17} \leftarrow 6_{16}$	7.5–6.5	3122.0276	–	−0.079
$7_{17} \leftarrow 6_{16}$	6.5–5.5	3122.0312	–	−0.030
$6_{15} \leftarrow 5_{14}$	–	3122.1323	0.0000	−0.054
$5_{23} \leftarrow 4_{22}$	5.5–4.5	3122.2470	–	−0.043
$5_{23} \leftarrow 4_{22}$	4.5–3.5	3122.2494	–	−0.052
$5_{32} \leftarrow 4_{31}$	–	3122.5179	0.0007	−0.030
$8_{08} \leftarrow 7_{07}$	–	3123.1751	–	−0.043
$6_{24} \leftarrow 5_{23}$	–	3123.4667	0.0028	−0.057

transitions like the components of the ortho-line $2_{12} \leftarrow 1_{01}$ (scanned in the range 91,280–91,400 MHz, with the OPO fixed at the rovibrational transition $2_{02} \leftarrow 1_{01}$ at 3116.535 cm^{-1} for DR) and the components of the para-line $3_{13} \leftarrow 2_{02}$ (scanned in the range 122,270–122,360 MHz, OPO fixed at $3_{03} \leftarrow 2_{02}$, 3117.656 cm^{-1}, for DR). Unfortunately, we did not detect any signal. We also applied another well-tried action spectroscopic method, in which the ternary attachment of He atoms at 4 K is used as an indicator for the rotational excitation of the bare ion [8,40–46]. Also here, we failed to detect the named lines.

Apart from some uncertainty of the predicted lines on the order of 10 MHz (see Table 3) and some uncertainty in the calculation of the centrifugal distortion and spin-rotation constants, one factor contributing to non-detection is that the trapped c-$C_3H_2^+$ ion ensemble is diluted with the linear $HCCCH^+$ structural isomer. As revealed by IR spectroscopy under very similar experimental

Table 2
The best fit of spectroscopic parameters for c-$C_3H_2^+$ obtained by fitting the rovibrational data with the program PGOPHER. All values are in MHz, and the uncertainties are given in parentheses in units of least significant figure.

Parameter	Ground state		ν_7	
	Calc.	Experimental	Calc.	Experimental
ν (cm^{-1})	…	…	3118.1[a]	3113.6400(3)
A_e	40269.0[b]			
B_e	30134.7[b]			
C_e	17236.2[b]			
A	40115.5[c]	40115.1(51)	40031.8[c]	40025.8(53)
B	29908.1[c]	29896.75(20)	29795.9[c]	29784.8(22)
C	17086.0[c]	17080.5(22)	17034.4[c]	17033.5(20)
Δ_N	0.04454[d]	0.0746(376)[f]	…	0.0746(376)[f]
Δ_{NK}	−0.04245[d]	−0.04245[g]	…	−0.04245[g]
Δ_K	0.1694[d]	0.1694[g]	…	0.1694[g]
δ_N	0.01801[d]	0.01801[g]		0.01801[g]
δ_K	0.03835[d]	0.03835[g]	…	0.03835[g]
ε_{aa}	141.636[e]	141.636[g]	…	141.636[g]
ε_{bb}	23.004[e]	23.004[g]	…	23.004[g]
ε_{cc}	−58.570[e]	−58.570[g]	…	−58.570[g]

[a] CCSD(T)/cc-pCVQZ harmonic frequency corrected by anharmonic contributions computed at the fc-CCSD(T)/cc-pVTZ level.
[b] Theoretical best estimates obtained using a composite scheme and basis set extrapolation techniques.
[c] Theoretical best estimates augmented by vibrational contributions obtained at the fc-CCSD(T)/cc-pVTZ level.
[d] Centrifugal distortion parameters calculated at CCSD(T)/cc-pCVQZ level of theory.
[e] Electron spin-rotation parameters calculated at fc-CCSD(T)/cc-pVTZ level of theory.
[f] Δ_N shared between ground and $\nu_7 = 1$ vibrational states.
[g] Fixed to theoretical values.

Table 3
Predicted frequencies of rotational transitions (in MHz, excluding hfs splitting) of c-$C_3H_2^+$ using the values in Table 2. Normalized intensities were calculated using PGOPHER with a 10 K rotational temperature. Only transitions with normalized intensity larger than 10^{-4} are listed.

$N'_{K'_aK'_c} \leftarrow N''_{K''_aK''_c}$	J'–J''	Frequency	Unc.	Norm. Intens. $\times 10^5$
$1_{10} \leftarrow 1_{01}$	1.5–1.5	23,084	5	19.5
$3_{21} \leftarrow 3_{12}$	2.5–2.5	43,978	9	12.7
$3_{21} \leftarrow 3_{12}$	3.5–3.5	44,085	9	17.2
$1_{11} \leftarrow 0_{00}$	1.5–0.5	57,216	6	14.9
$3_{30} \leftarrow 3_{21}$	3.5–3.5	62,837	29	10.7
$2_{21} \leftarrow 2_{12}$	1.5–1.5	68,951	16	12.2
$2_{21} \leftarrow 2_{12}$	2.5–2.5	69,201	16	19.0
$3_{12} \leftarrow 3_{03}$	2.5–2.5	75,361	11	13.6
$3_{12} \leftarrow 3_{03}$	3.5–3.5	75,510	11	18.4
$2_{02} \leftarrow 1_{11}$	2.5–1.5	76,962	8	14.0
$2_{12} \leftarrow 1_{01}$	2.5–1.5	91,352	8	71.4
$2_{12} \leftarrow 1_{01}$	1.5–0.5	91,354	8	39.7
$3_{03} \leftarrow 2_{12}$	3.5–2.5	117,000	9	78.6
$3_{03} \leftarrow 2_{12}$	2.5–1.5	117,068	9	55.0
$4_{23} \leftarrow 4_{14}$	4.5–4.5	120,791	19	11.5
$3_{13} \leftarrow 2_{02}$	3.5–2.5	122,295	10	28.8
$3_{13} \leftarrow 2_{02}$	2.5–1.5	122,331	10	20.2
$3_{12} \leftarrow 2_{21}$	3.5–2.5	123,308	18	15.8
$3_{12} \leftarrow 2_{21}$	2.5–1.5	123,478	18	11.1
$2_{21} \leftarrow 1_{10}$	1.5–0.5	137,371	16	48.3
$2_{21} \leftarrow 1_{10}$	2.5–1.5	137,469	16	86.9
$4_{04} \leftarrow 3_{13}$	4.5–3.5	153,142	9	25.8
$4_{04} \leftarrow 3_{13}$	3.5–2.5	153,200	9	19.9
$4_{14} \leftarrow 3_{03}$	4.5–3.5	154,559	10	78.9
$4_{14} \leftarrow 3_{03}$	3.5–2.5	154,610	10	60.8
$2_{20} \leftarrow 1_{11}$	1.5–0.5	156,868	14	11.7
$2_{20} \leftarrow 1_{11}$	2.5–1.5	157,037	14	21.1
$3_{22} \leftarrow 2_{11}$	2.5–1.5	171,551	16	15.0
$3_{22} \leftarrow 2_{11}$	3.5–2.5	171,602	16	21.3
$5_{05} \leftarrow 4_{14}$	5.5–4.5	187,812	10	54.5
$5_{05} \leftarrow 4_{14}$	4.5–3.5	187,869	10	44.4
$5_{15} \leftarrow 4_{04}$	5.5–4.5	188,130	10	18.2
$5_{15} \leftarrow 4_{04}$	4.5–3.5	188,185	10	14.8
$4_{23} \leftarrow 3_{12}$	3.5–2.5	199,832	15	32.6
$4_{23} \leftarrow 3_{12}$	4.5–3.5	199,840	15	42.2
$5_{14} \leftarrow 4_{23}$	5.5–4.5	218,054	10	22.3
$5_{14} \leftarrow 4_{23}$	4.5–3.5	218,117	10	18.2
$3_{31} \leftarrow 2_{20}$	2.5–1.5	220,772	26	19.7
$3_{31} \leftarrow 2_{20}$	3.5–2.5	220,901	26	28.1
$6_{16} \leftarrow 5_{05}$	6.5–5.5	222,135	16	29.8
$6_{16} \leftarrow 5_{05}$	5.5–4.5	222,191	16	25.1
$3_{30} \leftarrow 2_{21}$	2.5–1.5	230,092	23	57.2
$3_{30} \leftarrow 2_{21}$	3.5–2.5	230,231	23	81.6
$3_{21} \leftarrow 2_{12}$	2.5–1.5	236,407	15	17.5
$3_{21} \leftarrow 2_{12}$	3.5–2.5	236,595	15	24.9
$7_{07} \leftarrow 6_{16}$	7.5–6.5	256,230	30	13.0
$7_{07} \leftarrow 6_{16}$	6.5–5.5	256,287	30	11.3
$4_{32} \leftarrow 3_{21}$	3.5–2.5	256,824	27	29.1
$4_{32} \leftarrow 3_{21}$	4.5–3.5	256,920	27	37.6
$6_{25} \leftarrow 5_{14}$	6.5–5.5	258,143	17	11.7
$4_{41} \leftarrow 3_{30}$	3.5–2.5	303,670	35	36.1
$4_{41} \leftarrow 3_{30}$	4.5–3.5	303,807	35	46.8
$4_{40} \leftarrow 3_{31}$	3.5–2.5	307,092	33	12.1
$4_{40} \leftarrow 3_{31}$	4.5–3.5	307,229	33	15.6
$5_{41} \leftarrow 4_{32}$	4.5–3.5	365,330	29	12.2
$5_{41} \leftarrow 4_{32}$	5.5–4.5	365,455	29	14.9
$5_{50} \leftarrow 4_{41}$	4.5–3.5	386,122	44	12.6
$5_{50} \leftarrow 4_{41}$	5.5–4.5	386,261	44	15.4

conditions [15], electron impact ionization of allene produces a 60:40 ratio of the cyclic to the linear isomer. Also, further spectroscopic dilution of the signal very probably occurs by hyperfine splitting of the ortho-lines ($I = 1$). A renewed future search with deep integration at 4 K could benefit from a novel rotational-vibrational DR scheme recently tested in the Cologne group [39].

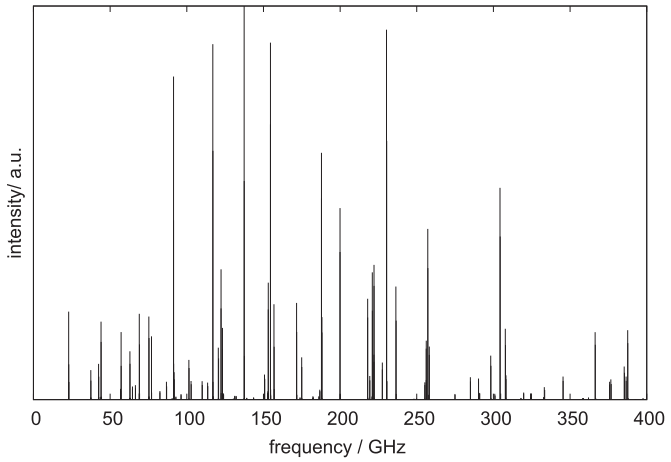

Fig. 4. Illustration of the expected rotational spectrum of c-$C_3H_2^+$ at $T = 10$ K, based on the spectroscopic parameters given in Table 2. The dipole moment of c-$C_3H_2^+$ is calculated at the CCSD(T)/cc-pCVQZ level to be 1.6 Debye.

8. Conclusions and outlook

This paper is the first exploitation of the LIHR-effect (Laser Induced Hindering of a Reaction) for high-resolution rovibrational spectroscopy. Applying this method in a cryogenic 22-pole ion trap by using reaction (1), ninety-one transitions have been measured for c-$C_3H_2^+$. Supported by high-level quantum chemical calculations, the ground state molecular parameters could be determined and thus the rotational spectrum of c-$C_3H_2^+$ predicted.

The details of the LIHR reaction mechanism are discussed elsewhere [16]. In brief, the reaction proceeds through a loosely bound complex in the entrance channel, whose lifetime is significantly reduced by the (vibrational) excitation of the reactants, and leading to a negative temperature dependence of the reaction rate coefficient [18]. This process enables the measurement of rovibrational spectra for species with similar reaction pathways, or, more generally speaking, for reactions with a negative temperature dependence. For c-$C_3H_2^+$ itself, it is very probable that LIHR-spectroscopy can also be performed for the symmetric CH-stretch ν_1 at 3139 cm^{-1} [15]. The situation is less clear for the structural isomer $HCCCH^+$, and it is an interesting question whether probing the antisymmetric IR active stretches ν_3 and ν_4 of $HCCCH^+$ at 3204 and 1899 cm^{-1} via this method will lead to any signal. Other potential target reactions are $NH_3^+ + H_2$ [47] and $CH_4^+ + H_2$ [48], which are known to have a negative temperature dependence at low temperature. Although the spectra of NH_3^+ and CH_4^+ are well understood, the general applicability of LIHR could be tested on these.

Unfortunately, the rotational spectrum of c-$C_3H_2^+$ could not be measured in this work. One reason contributing to this is the dilution of the signal due to fine structure and potentially hyperfine effects. These challenges will also apply to future searches of this ion in laboratory and space. A renewed laboratory search may profit from a novel double resonance scheme [39], which operates at a temperature of 4 K and thus yields an improved partition function.

Declaration of competing interest

The authors declare that they have no known competing financial interests or personal relationships that could have appeared to influence the work reported in this paper.

CRediT authorship contribution statement

Oskar Asvany: Supervision, Conceptualization, Investigation, Writing - original draft. **Charles R. Markus:** Investigation, Formal analysis, Writing - original draft. **Thomas Salomon:** Investigation. **Philipp C. Schmid:** Investigation, Writing - review & editing. **Shreyak Banhatti:** Investigation. **Sandra Brünken:** Conceptualization, Writing - review & editing. **Filippo Lipparini:** Formal analysis, Software, Writing - original draft. **Jürgen Gauss:** Formal analysis, Software, Writing - original draft. **Stephan Schlemmer:** Supervision, Conceptualization, Funding acquisition.

Acknowledgments

We dedicate this work to the memory of Jon T. Hougen. We remember him as someone very knowledgeable in science, very communicative, extremely entertaining, and speaking apparently nearly every language. He was also in strong support for the early stage researchers and did not care about hierarchies. When he once visited Cologne, it was impressive to see how he was interested in the work of the young PhD students, with whom he talked for hours in the lab.

This work has been supported by the Deutsche Forschungsgemeinschaft (DFG) via SFB 956 (project ID 184018867), subproject B2, grant AS 319/2-2 as wells as grant SCHL 341/15-1 (*"Cologne Center for Terahertz Spectroscopy"*) and GA 370/6-2 within the framework of the priority program SPP 1573. C. R. M. is grateful for support from the NASA Earth and Space Science Fellowship (NESSFNX16AO86H). S. Br. gratefully acknowledges the Netherlands Organisation for Scientific Research (NWO) for support of this work under project number 740.018.010. S. Ba. is supported by the H2020-MSCA-ITN-2016 Program (EUROPAH project, G. A. 722346). The authors gratefully acknowledge the work done over the last years by the electrical and mechanical workshops of the I. Physikalisches Institut.

References

[1] B. Turner, E. Herbst, R. Terzieva, The physics and chemistry of small translucent molecular clouds. XIII. The basic hydrocarbon chemistry, Astrophys. J. Suppl. Ser. 126 (2) (2000) 427–460, https://doi.org/10.1086/313301.
[2] J.-C. Loison, J. Cernicharo, N. Marcelino, M. Agndez, P. Gratier, V. Wakelam, D.N. Reyes, E. Roueff, M. Gerin, The interstellar chemistry of C_3H and C_3H_2 isomers, Mon. Not. Roy. Astron. Soc. 470 (4) (2017) 4075–4088.
[3] C.A. Gottlieb, J.M. Vrtilek, E.W. Gottlieb, P. Thaddeus, A. Hjalmarson, Laboratory detection of the C_3H radical, Astrophys. J. Lett. 294 (1985) L55–L58.
[4] P. Thaddeus, C.A. Gottlieb, A. Hjalmarson, L.E.B. Johansson, W.M. Irvine, P. Friberg, R.A. Linke, Astronomical identification of the C_3H radical, Astrophys. J. Lett. 294 (1985) L49–L53.
[5] S. Yamamoto, S. Saito, M. Ohishi, H. Suzuki, S.-I. Ishikawa, N. Kaifu, A. Murakami, Laboratory and astronomical detection of the cyclic C_3H radical, Astrophys. J. Lett. 322 (1987) L55.
[6] J. Cernicharo, C.A. Gottlieb, M. Guelin, T.C. Killian, G. Paubert, P. Thaddeus, J.M. Vrtilek, Astronomical detection of H_2CCC, Astrophys. J. Lett. 368 (1991) L39.
[7] J.M. Vrtilek, C.A. Gottlieb, P. Thaddeus, Laboratory and astronomical spectroscopy of C_3H_2, the first interstellar organic ring, Astrophys. J. Lett. 314 (1987) 716.
[8] S. Brünken, L. Kluge, A. Stoffels, O. Asvany, S. Schlemmer, Laboratory rotational spectrum of l-C_3H^+ and confirmation of its astronomical detection, Astrophys. J. Lett. 783 (2014) L4.
[9] J. Pety, P. Gratier, V. Guzmán, E. Roueff, M. Gerin, J.R. Goicoechea, S. Bardeau, A. Sievers, F. Le Petit, J. Le Bourlot, A. Belloche, D. Talbi, The IRAM-30 m line survey of the Horsehead PDR. II. First detection of the l-C_3H^+ hydrocarbon cation, A&A 548 (2012) A68.
[10] D. Zhao, K.D. Doney, H. Linnartz, Laboratory gas-phase detection of the cyclopropenyl cation (c-$C_3H_3^+$), Astrophys. J. Lett. 791 (2) (2014) L28.
[11] H. Clauberg, P. Chen, Geometry of c-$C_3H_2^+$: Franck-Condon factors in photoionization are a sensitive probe of polyatomic ion structure, J. Phys. Chem. 96 (14) (1992) 5676–5678.
[12] P. Hemberger, B. Noller, M. Steinbauer, I. Fischer, C. Alcaraz, B.K. Cunha de Miranda, G.A. Garcia, H. Soldi-Lose, Threshold photoelectron spectroscopy of cyclopropenylidene, chlorocyclopropenylidene, and their deuterated isotopomeres, J. Phys. Chem. A 114 (42) (2010) 11269–11276.
[13] P. Jusko, S. Brünken, O. Asvany, S. Thorwirth, A. Stoffels, L. van der Meer, G. Berden, B. Redlich, J. Oomens, S. Schlemmer, The FELion cryogenic ion trap beam line at the FELIX free-electron laser laboratory: infrared signatures of primary alcohol cations, Faraday Discuss 217 (2019) 172–202.
[14] D. Oepts, A. van der Meer, P. van Amersfoort, The Free-Electron-Laser user facility FELIX, Infrared Phys. Technol. 36 (1995) 297–308.
[15] S. Brünken, F. Lipparini, A. Stoffels, P. Jusko, B. Redlich, J. Gauss, S. Schlemmer, Gas-Phase vibrational spectroscopy of the hydrocarbon cations l-C_3H^+, HC_3H^+, and c-$C_3H_2^+$: structures, isomers, and the influence of Ne-tagging, J. Phys. Chem. A 123 (37) (2019) 8053–8062.
[16] A manuscript describing the detailed reaction mechanism of LIHR is in preparation by the same authors.
[17] M.W. Wong, L. Radom, Thermochemistry and ion-molecule reactions of isomeric $C_3H_2^+$ cations, J. Am. Chem. Soc. 115 (1993) 1507–1514.
[18] I. Savić, D. Gerlich, Temperature variable ion trap studies of $C_3H_n^+$ with H_2 and HD, Phys. Chem. Chem. Phys. 7 (2005) 1026–1035.
[19] O. Asvany, S. Brünken, L. Kluge, S. Schlemmer, COLTRAP: a 22-pole ion trapping machine for spectroscopy at 4 K, Appl. Phys. B 114 (1–2) (2014) 203–211.
[20] O. Asvany, F. Bielau, D. Moratschke, J. Krause, S. Schlemmer, New design of a cryogenic linear RF multipole trap, Rev. Sci. Instrum. 81 (2010), 076102.
[21] I. Shavitt, R.J. Bartlett, Many-body Methods in Chemistry and Physics: MBPT and Coupled-Cluster Theory, Cambridge University Press, Cambridge, 2009.
[22] G.D. Purvis, R.J. Bartlett, A full coupledcluster singles and doubles model: the inclusion of disconnected triples, J. Chem. Phys. 76 (1982) 1910.
[23] K. Raghavachari, G.W. Trucks, J.A. Pople, M. Head-Gordon, A fifth-order perturbation comparison of electron correlation theories, Chem. Phys. Lett. 157 (1989) 479.
[24] T.H. Dunning Jr., Gaussian basis sets for use in correlated molecular calculations. i. the atoms boron through neon and hydrogen, J. Chem. Phys. 90 (1989) 1007.
[25] D.E. Woon, T.H. Dunning Jr., Gaussian basis sets for use in correlated molecular calculations. v. corevalence basis sets for boron through neon, J. Chem. Phys. 103 (1995) 4572.
[26] J.D. Watts, J. Gauss, R.J. Bartlett, Open-shell analytical energy gradients for triple excitation many-body, coupled-cluster methods: MBPT(4), CCSD+T(CCSD), CCSD(T),and QCISD(T), Chem. Phys. Lett. 200 (1992) 1.
[27] M. Heckert, M. Kállay, J. Gauss, Molecular equilibrium geometries based on coupled-cluster calculations including quadruple excitations, Mol. Phys. 103 (2005) 2109.
[28] M. Heckert, M. Kállay, D.P. Tew, W. Klopper, J. Gauss, Basis-set extrapolation techniques for the accurate calculation of molecular equilibrium geometries using coupled-cluster theory, J. Chem. Phys. 125 (2006), 044108.
[29] J. Gauss, J.F. Stanton, Analytic CCSD(T) second derivatives, Chem. Phys. Lett. 276 (1997) 70.
[30] P.G. Szalay, J. Gauss, J.F. Stanton, Analytic UHF-CCSD(T) second derivatives: implementation and application to the calculation of the vibration-rotation interaction constants of NCO and NCS, Theor. Chem. Acc. 100 (1998) 5.
[31] I.M. Mills, Vibration-rotation structure in asymmetric- and symmetric-top molecules, in: K.N. Rao, C.W. Mathews (Eds.), Molecular Spectroscopy: Modern Research, Academic Press, New York, 1972, p. 115.
[32] J.F. Stanton, C.L. Lopreore, J. Gauss, The equilibrium structure and fundamental vibrational frequencies of dioxirane, J. Chem. Phys. 108 (1998) 7190.
[33] G. Tarczay, P.G. Szalay, J. Gauss, First-principles calculation of electron spin-rotation tensors, J. Phys. Chem. A 114 (2010) 34.
[34] J. F. Stanton, J. Gauss, L. Cheng, M. E. Harding, D. A. Matthews, P. G. Szalay, CFOUR, Coupled-Cluster techniques for Computational Chemistry, a quantum-chemical program package, With contributions from A.A. Auer, R.J. Bartlett, U. Benedikt, C. Berger, D.E. Bernholdt, Y.J. Bomble, O. Christiansen, F. Engel, R. Faber, M. Heckert, O. Heun, M. Hilgenberg, C. Huber, T.-C. Jagau, D. Jonsson, J. Jusélius, T. Kirsch, K. Klein, W.J. Lauderdale, F. Lipparini, T. Metzroth, L.A. Mück, D.P. O'Neill, D.R. Price, E. Prochnow, C. Puzzarini, K. Ruud, F. Schiffmann, W. Schwalbach, C. Simmons, S. Stopkowicz, A. Tajti, J. Vázquez, F. Wang, J.D. Watts and the integral packages MOLECULE (J. Almlöf and P.R. Taylor), PROPS (P.R. Taylor), ABACUS (T. Helgaker, H.J. Aa. Jensen, P. Jørgensen, and J. Olsen), and ECP routines by A. V. Mitin and C. van Wüllen. For the current version, see http://www.cfour.de.
[35] C. Western, Pgopher: a program for simulating rotational, vibrational and electronic spectra, J. Quant. Spectrosc. Radiat. Transf. 186 (2017) 221–242.
[36] S. Gärtner, J. Krieg, A. Klemann, O. Asvany, S. Brünken, S. Schlemmer, High-resolution spectroscopy of CH_2D^+ in a cold 22-Pole ion trap, J. Phys. Chem. A 117 (39) (2013) 9975–9984.
[37] M. Töpfer, P. Jusko, S. Schlemmer, O. Asvany, Double resonance rotational spectroscopy of CH_2D^+, Astron. Astrophys. 593 (2016) L11.
[38] M. Töpfer, T. Salomon, S. Schlemmer, O. Dopfer, H. Kohguchi, K.M.T. Yamada, O. Asvany, Double resonance rotational spectroscopy of Weakly Bound Ionic Complexes: the case of floppy CH_3^+-He, Phys. Rev. Lett. 121 (2018), 143001.
[39] C. Markus, S. Thorwirth, O. Asvany, S. Schlemmer, High-resolution double resonance action spectroscopy in ion traps: vibrational and rotational fingerprints of $CH_2NH_2^+$, Phys. Chem. Chem. Phys. 21 (2019) 26406–26412.
[40] A. Stoffels, L. Kluge, S. Schlemmer, S. Brünken, Laboratory rotational ground state transitions of NH_3D^+ and CF^+, Astron. Astrophys. 593 (2016) A56.
[41] J.L. Doménech, S. Schlemmer, O. Asvany, Accurate frequency determination of vibration-rotation and rotational transitions of SiH^+, Astrophys. J. 849 (2017) 60.

[42] J.L. Doménech, P. Jusko, S. Schlemmer, O. Asvany, The first laboratory detection of vibration-rotation transitions of $^{12}CH^+$ and $^{13}CH^+$ and improved measurement of their rotational transition frequencies, Astrophys. J. 857 (2018) 61.
[43] J.L. Doménech, S. Schlemmer, O. Asvany, Accurate rotational rest frequencies for ammonium ion isotopologues, Astrophys. J. 866 (2) (2018) 158.
[44] T. Salomon, M. Töpfer, P. Schreier, S. Schlemmer, H. Kohguchi, L. Surin, O. Asvany, Double resonance rotational spectroscopy of He-HCO^+, Phys. Chem. Chem. Phys. 21 (2019) 3440–3445.
[45] S. Thorwirth, P. Schreier, T. Salomon, S. Schlemmer, O. Asvany, Pure rotational spectrum of CN^+, Astrophys. J. 882 (1) (2019) L6.
[46] S. Brünken, L. Kluge, A. Stoffels, J. Perez-Rios, S. Schlemmer, Rotational state-dependent attachment of He atoms to cold, molecular ions: An action spectroscopic scheme for rotational spectroscopy, J. Mol. Spectrosc. 332 (2017) 67–78.
[47] E. Herbst, D.J. DeFrees, D. Talbi, F. Pauzat, W. Koch, A.D. McLean, Calculations on the rate of the ionmolecule reaction between NH_3^+ and H_2, J. Chem. Phys. 94 (12) (1991) 7842–7849.
[48] O. Asvany, I. Savić, S. Schlemmer, D. Gerlich, Variable temperature ion trap studies of $CH_4^+ + H_2$, HD and D_2: negative temperature dependence and significant isotope effect, Chem. Phys. 298 (2004) 97–105.